

RESEARCH ARTICLE

Open Access



Maize *male sterile 33* encodes a putative glycerol-3-phosphate acyltransferase that mediates anther cuticle formation and microspore development

Lei Zhang^{1†}, Hongbing Luo^{2†}, Yue Zhao^{1†}, Xiaoyang Chen¹, Yumin Huang¹, Shuangshuang Yan³, Suxing Li¹, Meishan Liu¹, Wei Huang¹, Xiaolan Zhang³ and Weiwei Jin^{1*}

Abstract

Background: The anther cuticle, which is primarily composed of lipid polymers, is crucial for pollen development and plays important roles in sexual reproduction in higher plants. However, the mechanism underlying the biosynthesis of lipid polymers in maize (*Zea mays* L.) remains unclear.

Results: Here, we report that the maize male-sterile mutant *shrinking anther 1 (sa1)*, which is allelic to the classic mutant *male sterile 33 (ms33)*, displays defective anther cuticle development and premature microspore degradation. We isolated *MS33* via map-based cloning. *MS33* encodes a putative glycerol-3-phosphate acyltransferase and is preferentially expressed in tapetal cells during anther development. Gas chromatography-mass spectrometry revealed a substantial reduction in wax and cutin in *ms33* anthers compared to wild type. Accordingly, RNA-sequencing analysis showed that many genes involved in wax and cutin biosynthesis are differentially expressed in *ms33* compared to wild type.

Conclusions: Our findings suggest that *MS33* may contribute to anther cuticle and microspore development by affecting lipid polyester biosynthesis in maize.

Keywords: Maize, Male sterile, MS33, Anther cuticle, Tapetum, GPAT

Background

The pollen grains of angiosperms are produced in the anther compartment of the flower stamen. In maize, each male floret has three anthers, each with four lobes. These four lobes have similar structures and are attached to a central core connected to the vascular tissue. After morphogenesis, each anther differentiates into a four-layered structure. From the exterior to the interior, the centrally located microspores are covered by the epidermis, endothecium, middle layer, and tapetum [1, 2].

Male gametophyte development requires the functional cooperation of gametophytic and sporophytic tissues. The tapetum contributes to microspore development by providing energy and structural materials [3–5]. Mature pollen is covered by a complex exine, which is highly resistant to physical and chemical degradation and thus protects male gametophytes against drought, irradiation, and other environmental stresses [6–8]. The main component of the pollen exine is sporopollenin, a biopolymer formed by lipid monomers covalently coupled by ether and ester linkages. The major lipid precursors of sporopollenin include straight-chain fatty acids and oxygenated aromatic monomers, such as p-coumaric (C9) and ferulic (C10) acids, all of which are synthesized in the tapetum. After meiosis in the anther is complete, sporopollenin is secreted by the tapetum, transported to the microspore surface, and used for pollen exine formation [9, 10].

* Correspondence: weiweijin@cau.edu.cn

[†]Lei Zhang, Hongbing Luo and Yue Zhao contributed equally to this work.

¹National Maize Improvement Center of China, Beijing Key Laboratory of Crop Genetic Improvement, Key Laboratory of Crop Heterosis and Utilization, Ministry of Education (MOE), Center for Crop Functional Genomics and Molecular Breeding, China Agricultural University, Beijing 100193, China
Full list of author information is available at the end of the article



The epidermis of the anther is covered by the cuticle, a chemically stable layer that protects anthers from dehydration during development [8, 11]. Like the surface layers of vegetative organs, such as leaves and stems, the anther cuticle comprises two types of lipophilic biopolymers, cutin and wax. Cutin is composed of hydroxylated and epoxy C16 and C18 fatty acids, and wax is mainly formed by long-chain fatty acids [6, 9, 10, 12, 13]. The biosynthetic pathway of cutin has been elucidated gradually in recent researches, which consist of monomer synthesis, export and polymerization [14, 15]. The cutin monomers are synthesized from the plastid-derived 16C and 18C fatty acids in the endoplasmic reticulum, with the esterification of long-chain acyl-CoA synthetases (LACS) and the oxidation of cytochrome P450 oxidases from the CYP86 and CYP77 subfamilies [15, 16]. Then, the mature monoacylglycerol cutin monomers are generated by transfer of the acyl group from acyl-CoA to glycerol-3-phosphate under the catalysis of GPAT. The ABC transporters export the cutin monomers from endoplasmic reticulum to the site of polymerization [15]. Wax biosynthesis begins with a de novo C16 or C18 fatty acid in the plastid. Then, the LACS catalyze the long-chain fatty acid compounds to C16 or C18 acyl-CoA and then transferred to the endoplasmic reticulum. The fatty acid elongase (FAE) complex catalyze the C16 or C18 acyl-CoA to very-long-chain fatty acids (VLCFAs) with predominant chain lengths ranging from 24 to 36 carbons through several cycles of reaction. The aliphatic wax constituents are generated from VLCFAs by the alcohol-forming pathways, which give rise to primary alcohols and wax eaters, and the alkane-forming pathways, which produce aldehydes, alkanes, secondary alcohols, and ketones [17, 18].

In recent years, many genes have been identified to contribute to anther cuticle and pollen exine development, such as *AMS1* (*ABORTED MICROSPORES*) [7], *MS1* (*MALE STERILITY1*) [19], *MS2* (*MALE STERILITY2*) [20], *FLP1* (*FACELESS POLLEN1*) [21], *DEX1* (*DEFECTIVE IN EXINE PATTERN FORMATION1*) [22], *NEF1* (*NO EXINE FORMATION1*) [23], *CYP703A2* [24], *ACOS5* (*ACYL-COA SYNTHETASE5*) [25], and *CYP704B1* [26] in *Arabidopsis thaliana*, as well as the rice genes *TDR* (*TAPETUM DEGENERATION RETARDATION*) [27], *GAMYB* [28], *PDA1* (*POST-MEIOTIC DEFICIENT ANTHER1*) [29], *PTC1* (*PERSISTENT TAPETAL CELL1*) [30], *OsC6* [31], *WDA1* (*WAX-DEFICIENT ANTHER1*) [32], *CYP703A3* [10], *CYP704B2* [33], and *NPI* (*NO POLLEN1*) [34]. These genes are involved in fatty acid biosynthesis, modification, transport, and metabolism. Mutations in these genes result in abortion of the male gamete. However, the role of fatty acids in polyester formation is currently unclear [7, 9, 10].

In *Arabidopsis*, several glycerol-3-phosphate acyltransferase (GPAT) family members have been shown to participate in epidermal polyester formation in vegetative tissues [8]. GPAT catalyzes the esterification of a fatty acyl from acyl-CoA to the sn-2 position of glycerol-3-phosphate (G3P), producing lysophosphatidate (LPA). LPA is a substrate for lipid monomer biosynthesis during cutin and wax production in plants [35]. Genetic analysis suggested that GPAT is involved in pollen development in *Arabidopsis*. For example, the *gpac1* mutant exhibits anomalous pollen coat structure and very poor male fertility, and the *gpac1 gpac6* double mutant is completely male sterile [36]. One GPAT family member, OsGPAT3, plays a critical role in anther cuticle and male gamete development in rice [37]. However, whether GPATs directly participate in pollen development and polyester formation in the anther cuticle in maize remains unknown.

Although many male-sterile mutants in maize are available, very few of them have been functionally characterized [38]. *MS26* [39] and *MS45* [40], which have been functionally characterized, are required for pollen wall development. *MS26*, a homolog of *CYP704B1* in *Arabidopsis* and *CYP704B2* in rice, encodes a putative cytochrome P450 mono-oxygenase [41] that participates in the ω -hydroxylation of C16 and C18 fatty acids [26, 42]. *MS45*, which is expressed in the tapetal layer, encodes a putative strictosidine synthase involved in alkaloid biosynthesis [43, 44]. Maize *IPE1* (*IRREGULAR POLLEN EXINE1*), encoding a putative glc-methanol-choline oxidoreductase, participates in the oxidative pathway of C16/C18 ω -hydroxy fatty acids. *IPE1*, *MS26*, and *MS45* might cooperatively mediate anther cuticle and pollen exine development [45]. The maize *CYP703A2* subfamily member, *APV1* (*ABNORMAL POLLEN VACUOLATION1*), also participates in the fatty acid hydroxylation pathway, which contributes to the biosynthesis of cutin monomers and sporopollenin precursors [46].

Here, we identified the maize male-sterile mutant *shrinking anther 1* (*sa1*), which displays abnormal tapetum and anther cuticle development. Allelism tests confirmed that *sa1* is allelic to the classical maize male sterile mutant *ms33*. However, the *MS33* gene has not yet been cloned. In the current study, we used map-based cloning to isolate the *MS33* gene and found that it encodes a putative GPAT. *MS33* was temporally expressed in the tapetum during anther development. The anthers of the *MS33* mutant had substantially reduced cutin and wax contents compared to wild type. Additionally, transcriptomic analysis revealed differentially expressed genes (DEGs) involved in wax, cutin, and fatty acid biosynthesis. Our findings suggest that *MS33* may play an essential role in anther cuticle and pollen grain development in maize.

Results

Characterization of the male-sterile mutant *sa1*

A male-sterile mutant, *shrinking anther 1* (*sa1*), was identified by screening a *MuDR* library [47]. This mutant exhibited normal vegetative development (Fig. 1a), whereas the anthers, which were not extruded from the spikelets, were small and wilted and failed to produce pollen grains (Fig. 1c, e, g, i). When *sa1* was pollinated by wild-type plants, seed production was normal and all F_1 plants were fertile. The F_2 plants showed a phenotype segregation ratio of 3:1 (fertile: sterile = 153:55, $\chi^2 < \chi^2(0.05, 1) = 3.84$). These data suggest that female fertility is not affected in *sa1* and that its phenotype is due to a single recessive gene.

To further examine the defects in *sa1*, we examined semi-thin transverse sections to compare the cytology of wild-type versus *sa1* anthers and found no difference in anatomical structure or meiotic events in the wild-type and *sa1* plants before the tetrad stage (Fig. 2a, b, c, h, i, j). The *sa1* anthers contained four somatic layers, and

meiocytes were able to undergo normal meiosis II to form detectable tetrads (Fig. 2j).

At the early uninucleate stage, wild-type anthers had a thin middle layer, and the tapetum was degraded and appeared highly condensed (Fig. 2d). However, in *sa1*, the tapetal layer became thinner (Fig. 2k), pointing to more severe degradation of the tapetum. At the late uninucleate microspore stage, in wild-type anthers, the middle layer disappeared and the tapetal layer was degraded continuously but remained visible. Microspores, which contained full cytoplasm, gradually enlarged and became rounded (Fig. 2e). By contrast, in *sa1* anthers, the tapetum was almost completely degraded and barely any cellular material remained (Fig. 2l). This degeneration resembled that observed in *ipe1* [45]. The microspores of *sa1* appeared irregular. In wild-type plants, the tapetal layer exhibited a strip-like shape at the binucleate stage, and the microspores were still vacuolated (Fig. 2f). By contrast, in *sa1* anthers, the anther layers appeared collapsed and the microspores were defective (Fig. 2m). At

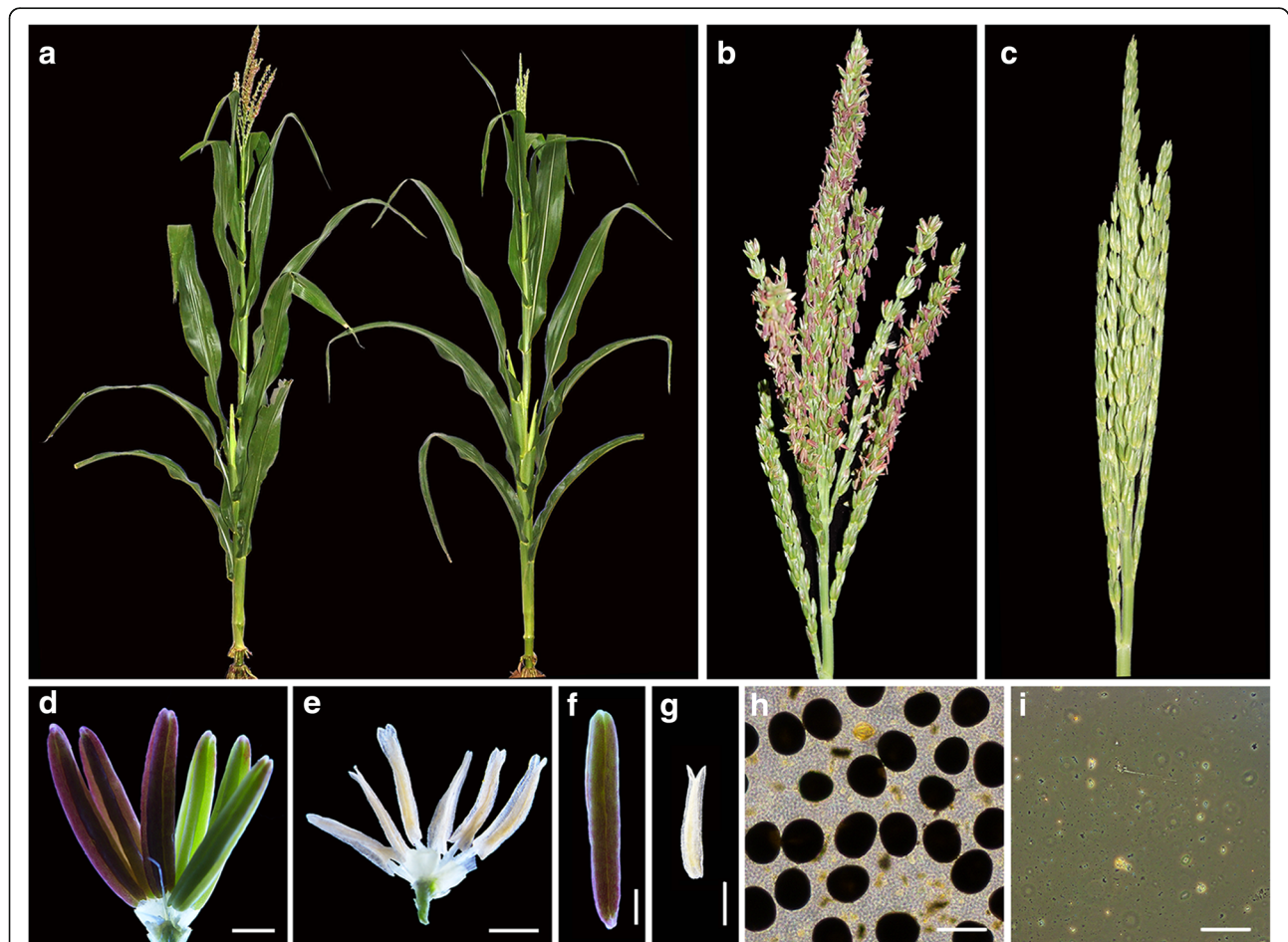


Fig. 1 Phenotypic comparison of wild-type and *sa1* plants. **(a)** Wild-type plant (left) and *sa1* plant (right). **(b)** Wild-type inflorescence. **(c)** *sa1* inflorescence. **(d)** Wild-type flower. **(e)** *sa1* flower. **(f)** Wild-type anther. **(g)** *sa1* anther. **(h)** Viable pollen grains from a wild-type plant after I_2 -KI staining. **(i)** Nonviable pollen grains from an *sa1* plant after I_2 -KI staining. Bar = 1 mm in **(d)**, **(e)**, **(f)**, and **(g)**, 50 μ m in **(h)** and **(i)**

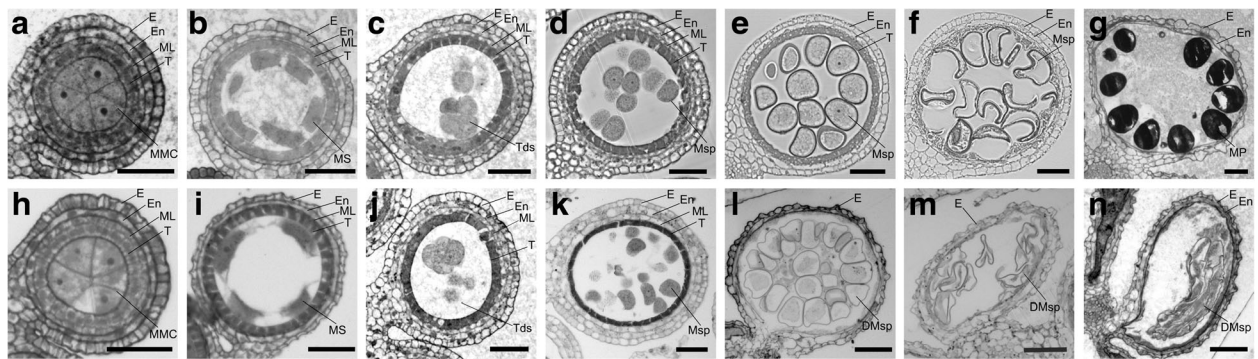


Fig. 2 Transverse sections showing anther development in wild-type and *sal1* plants. Transverse sections of wild-type anthers are shown in a-g, and those of *sal1* anthers are shown in h-n. (a) and (h), premeiosis stage. (b) and (i), meicyte stage. (c) and (j), tetrad stage. (d) and (k), early uninucleate stage. (e) and (l), late uninucleate stage. (f) and (m), binucleate stage. (g) and (n), mature pollen grain stage. DMsp, degenerated microspores; E, epidermis; En, endothecium; ML, middle layer; MMC, microspore mother cell; Mp, mature pollen; Ms, meiospores; Msp, microspore; T, tapetum; Tds, tetrads. Bars = 50 μ m

the mature pollen grain stage, in wild-type anthers, many pollen grains were present in the anther locule (Fig. 2g), whereas in *sal1* anthers, no pollen grains were observed, and only some residual debris remained (Fig. 2n). These phenotypes suggest that SA1 may be involved in tapetum degradation and microspore development during anther development.

SA1 is crucial for microspore and anther cuticle development

Transmission electron microscopy (TEM) revealed that at the early uninucleate microspore stage, wild-type tapetal cells contained numerous subcellular organelles, and Ubisch bodies were clearly visible in the inner surface of tapetum (Fig. 3a, c, e). However, in *sal1* plants, almost all subcellular organelles were degenerated, although Ubisch bodies were visible. Unlike the circular microspores of the wild type, *sal1* microspores were irregular in shape (Fig. 3b, d, f, g, h). At the late uninucleate microspore stage, the *sal1* tapetum was severely degraded, and no subcellular organelles or lipid bodies were observed (Fig. 3i, j, k, l). Ubisch bodies, which act as transporters for sporopollenin precursors between microspores and the tapetum, were slightly degraded in the *sal1* mutant (Fig. 3m, n). In addition, compared with the wild-type microspores, the *sal1* microspores were severely collapsed at this stage (Fig. 3o, p). At the binucleate microspore stage, the Ubisch bodies were degenerated in wild-type anthers and completely absent in *sal1* anthers (Fig. 3s, t). These results further indicate that SA1 may play crucial roles in microspore development and tapetal degradation.

We then used scanning electron microscopy (SEM) to further investigate anther cuticle formation in *sal1* plants. At the late binucleate microspore stage, the cuticular ridges showed a stereoscopic knitting-like pattern in the wild-type plants (Fig. 4a, c). However, in the *sal1* mutant, the

anther epidermis was smooth, with no obvious ridges; the anther epidermis had a slightly shrunken appearance (Fig. 4b, d). At the mature pollen grain stage, abundant pollen grains were observed in the wild type, whereas no pollen grains were detected in *sal1* anthers (Fig. 4e, f). In wild-type plants, reticulate cuticle covered the outermost surface and abundant Ubisch bodies were distributed on the outside of tapetal cells. By contrast, the outer surfaces of *sal1* anthers were glossy, and no Ubisch bodies were detected on the inner surface (Fig. 4g, h, i, j). These results suggest that anther cuticle development was disrupted in *sal1*.

Map-based cloning of SA1

We performed map-based cloning to isolate the *SA1* gene using 273 male-sterile plants from a segregating F_2 population. *SA1* was initially mapped to a 1.84-Mb interval between two markers, *umc1736* and *umc2214*, on chromosome 2 (Fig. 5a). Then, a number of InDel markers were developed for fine mapping using 2871 mutant individuals from the F_2 population. The target region, including nine predicted open reading frames (ORFs), was narrowed down to a 190-kb interval between markers *IDP607* and *IDP647* (Fig. 5a). One of the nine ORFs, *GRMZM2G070304*, which spans 2161 bp and has two exons and one intron, encodes a putative GPAT with 525 amino acids. Sequence analysis of *sal1* genomic DNA revealed a 247-bp insertion in the second exon of *GRMZM2G070304* (Fig. 5b).

In a previous study, another recessive male-sterile mutant, *ms33*, was also mapped near this region, but the gene was not isolated [38]. The phenotype of *ms33* is very similar to that of *sal1* [48]. Therefore, we performed an allelism test to determine whether *ms33* is allelic to *sal1*. A *sal1* homozygote was pollinated by a fertile heterozygote (+/*ms33*) from the *ms33-6019* allelic line. The progeny exhibited a fertile: sterile segregation ratio of

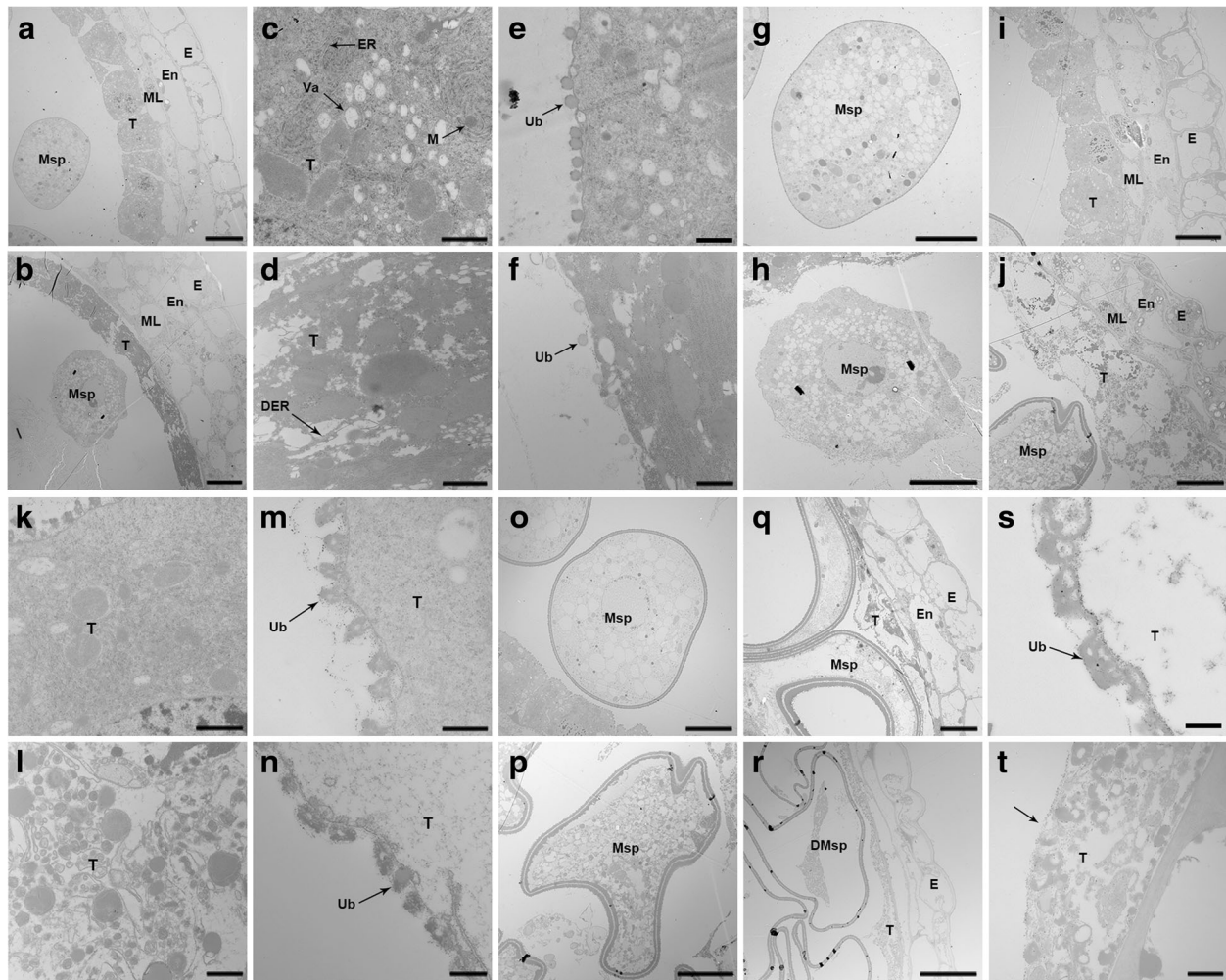


Fig. 3 Transmission electron microscopy of anthers from wild-type and *sa1* plants. Early uninucleate stage anthers are shown in (a) to (h): wild-type (a) and *sa1* anthers (b); tapetal layers in wild type (c) and *sa1* (d); Ubisch bodies in wild type (e) and *sa1* (f); Microspores in wild type (g) and *sa1* (h). Late uninucleate stage anthers are shown in (i) to (p): wild-type (i) and *sa1* anthers (j); tapetal layers in wild type (k) and *sa1* (l); Ubisch bodies in wild type (m) and *sa1* (n); microspores in wild type (o) and *sa1* (p). Binucleate stage anthers are shown in (q) to (t): wild-type (q) and *sa1* anthers (r); Ubisch bodies in wild type (s) and *sa1* (t). Bar = 10 μm in (a), (b), (g), (h), (i), (j), (o), (p), (q), and (r); 1 μm in (c), (d), (k), and (l); 500 nm in (e), (f), (m), (n), (s), and (t). DER, degenerated endoplasmic reticulum; DMsp, degenerated microspores; E, epidermis; En, endothecium; ER, endoplasmic reticulum; M, mitochondria; ML, middle layer; Msp, microspores; T, tapetal layer; Ub, Ubisch body; Va, vacuole

1:1, suggesting that *ms33* is allelic to *sa1*. Sequencing analysis revealed that *ms33-6019* had a 479-bp deletion in the first exon of *GRMZM2G070304* (Fig. 5b).

We also sequenced *GRMZM2G070304* from two additional *ms33* allelic lines: *ms33-6024* and *ms33-6038*. In *ms33-6024*, two base pairs were inserted at the 507th base pair from the translational start site of this gene, and there was a 5 base-pair deletion at the beginning of the second intron. In *ms33-6038*, one base pair was inserted after the 371th base pair. Bioinformatic analysis predicted that these mutations in *ms33-6024* and *ms33-6038* might result in a frameshift and premature translational termination. These results suggest that the *sa1/ms33* phenotype is likely caused by the mutations in *GRMZM2G070304*.

Phylogenetic analysis of MS33

GPATs have been characterized in bacteria, fungi, animals, and plants. These enzymes catalyze the transfer of an acyl group from acyl-CoA/ACP to the sn-1/2 position of glycerol-3-phosphate (G3P), i.e., the first step of de novo synthesis of membrane and storage lipids [49]. In *Arabidopsis*, 10 genes encoding GPAT enzymes have been annotated. GPAT1–GPAT8 clustered together in a single family based on sequence similarity analysis. This family has been found only in land plant species and shows sn-2 catalytic activity [8].

To identify the GPAT family members in maize and to explore the evolutionary role of MS33, we used the 10 *Arabidopsis* GPAT protein sequences as queries to search for their homologs in the maize and rice genomes

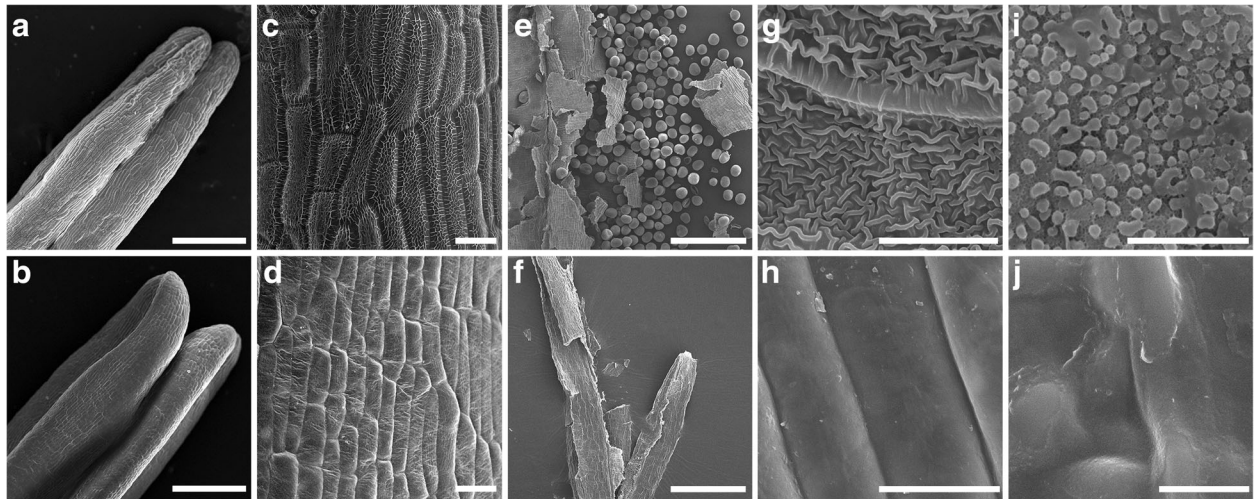


Fig. 4 Scanning electron microscopy of wild-type and *sa1* anthers at binucleate and mature pollen grain stages. **(a)** and **(b)** The epidermal surfaces of a wild-type **(a)** and *sa1* anthers **(b)** at the binucleate stage. Bar = 250 μ m. **(c)** and **(d)** Enlarged detailed view of the epidermal surfaces of anthers in wild type **(c)** and *sa1* **(d)** at the binucleate stage. Bar = 20 μ m. **(e)** and **(f)** Many mature pollen grains are visible in wild type **(e)**, but none are visible in *sa1* **(f)** at the mature pollen grain stage. Bar = 500 μ m. **(g)** to **(j)** The outer **(g)** and inner **(i)** surfaces of wild-type anthers compared to the outer **(h)** and inner **(j)** surfaces of *sa1* anthers. The outer surface of the *sa1* anther is glossy **(h)**, and no Ubisch bodies are visible on the inner anther surface **(j)**. Bar = 10 μ m in **(g)** and **(h)**, 5 μ m in **(i)** and **(j)**

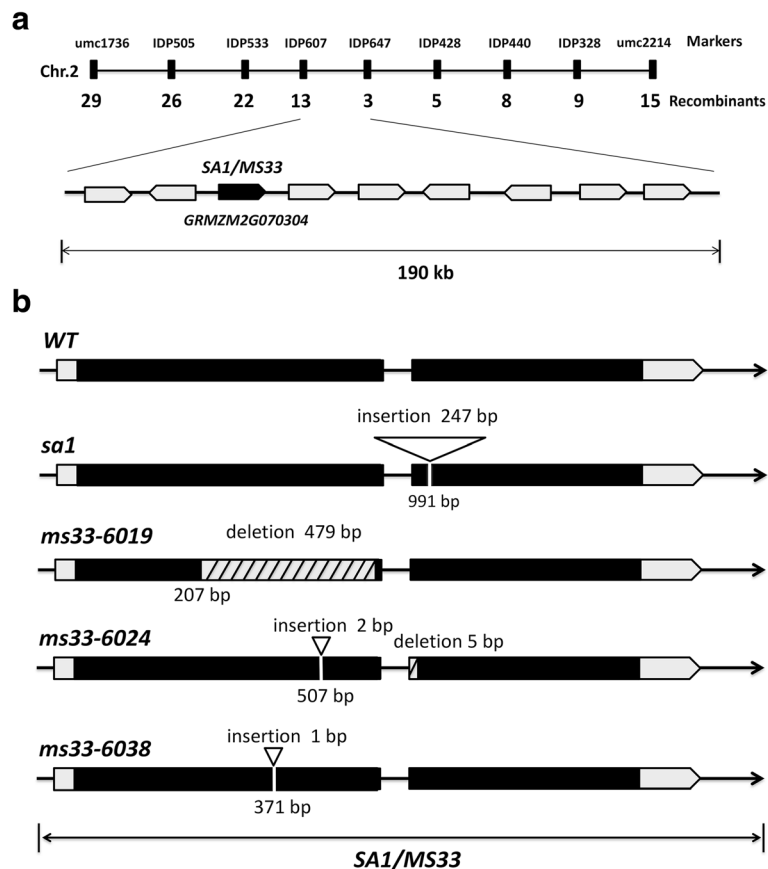


Fig. 5 Map-based cloning and gene structure of *SA1/MS33*. **(a)** Fine mapping of the *SA1* gene on chromosome 2. Molecular markers and genes in the mapping region are indicated **(b)** Schematic representation of the structure of maize *SA1* in the wild type, *sa1*, *ms33-6019*, *ms33-6024*, and *ms33-6038*

by BLASTP against the Gramene database. Overall, 20 maize GPAT homologs including MS33 and 17 putative rice GPATs were identified. A neighbor-joining phylogenetic tree was then constructed (Additional file 1: Figure S1). The result shows that SA1/MS33 shares the highest similarity with rice Os11g45400. Both of them were clearly classified into the GPAT2/3 group.

Expression pattern of MS33

To further explore the function of MS33, we performed quantitative PCR (qPCR) analysis using total RNA extracted from various organs of wild-type plants. The qPCR assay detected MS33 transcripts in all tissues examined, including anther, root, stem, and leaf tissue. Notably, MS33 expression was dramatically stimulated in developing anthers, reaching a peak at the tetrad stage (Fig. 6a).

We then performed RNA in situ hybridization to investigate the spatiotemporal expression pattern of MS33. Strong MS33 expression was detected in the tapetum from pre-meiosis to the binucleate stage (Fig. 6b-f). In the controls, no signal was detected when MS33 sense probe was used (Fig. 6g). Similarly, previous studies have shown that MS45 is specifically expressed in tapetal cells during early microspore development [38]. These expression patterns suggest that MS33 might be involved in the synthesis of aliphatic materials required for anther cuticle and microspore development.

The content and composition of cutin and wax are altered in *ms33* anthers

In *Arabidopsis*, GPATs participate in cutin and suberin biosynthesis. The levels of aliphatic polyester monomers

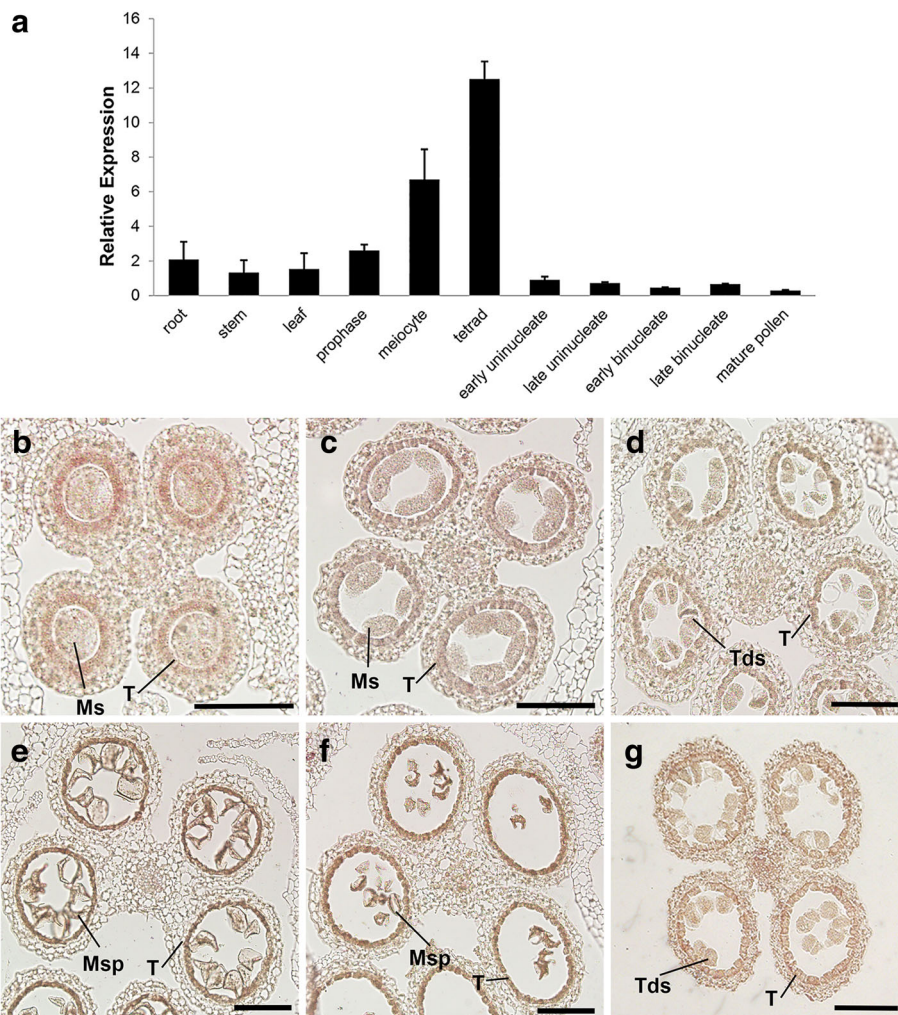
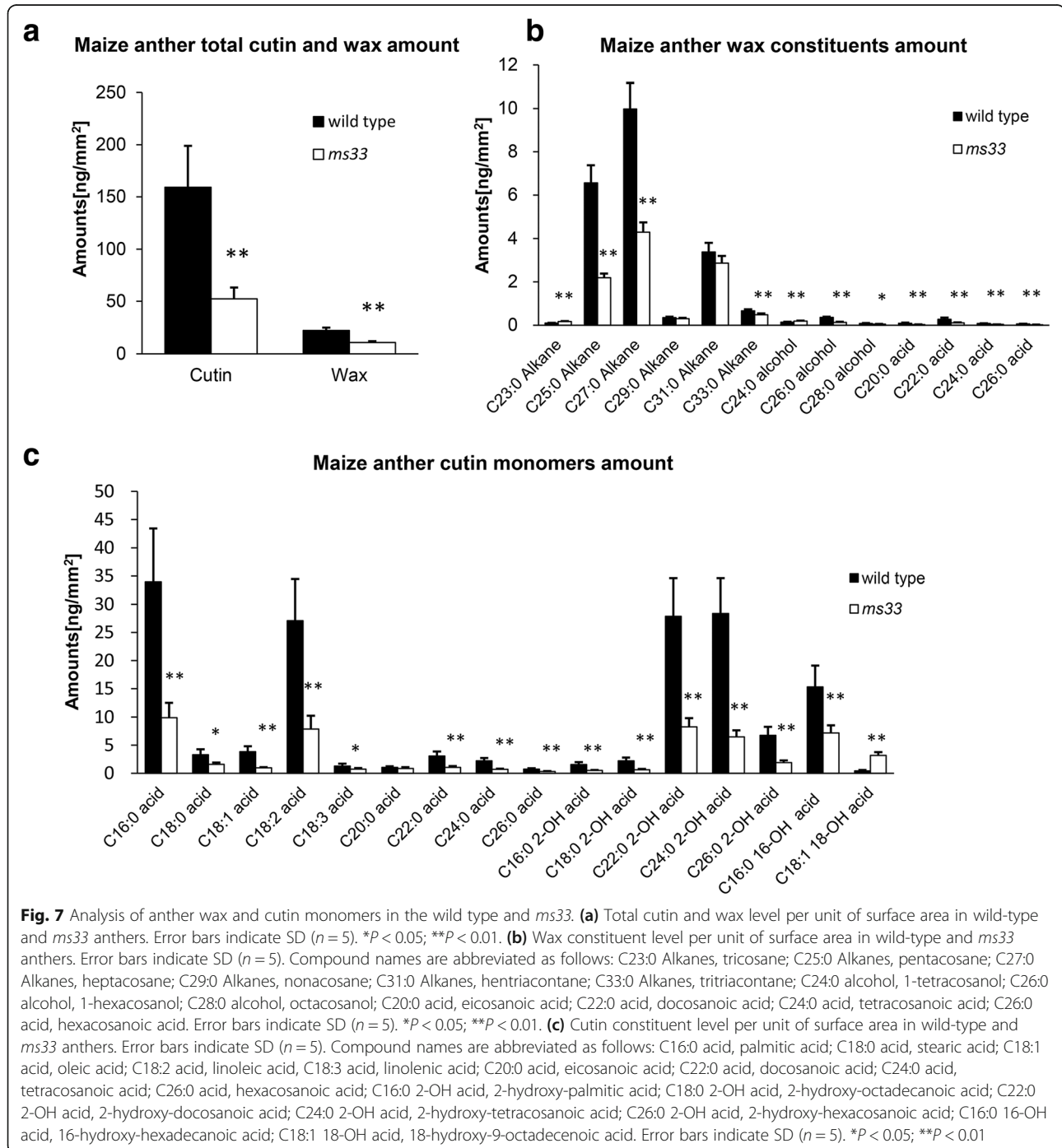


Fig. 6 Expression pattern of MS33. **(a)** qRT-PCR analysis of MS33 in different tissues and stages of pollen development. Data are presented as mean \pm SE ($n = 3$). **(b-g)** In situ analysis of MS33 expression in wild-type anthers. **(b) to (f)** MS33 is highly expressed in tapetal cells of anthers at the premeiosis **(b)**, meiocyte **(c)**, tetrad **(d)**, uninucleate **(e)**, and binucleate stages **(f)**. **(g)** anthers at tetrad stage hybridized with the MS33 sense probe. Ms, meiospores; Msp, microspore; T, tapetum; Tds, tetrads. Bars = 100 μ m

are greatly reduced in leaves, stems, and flowers of GPAT mutants [8]. To investigate whether MS33 is involved in polyester monomer biosynthesis in maize anthers, we performed gas chromatography-mass spectrometry to measure the composition of aliphatic monomers in wild-type and *ms33* anthers.

As shown in Fig. 7a, compared to wild-type anthers, total wax and cutin levels were significantly reduced in *ms33* anthers (by 51 and 67%, respectively). Among wax

components, the amounts of the two predominate monomers in anthers, C25 and C27 alkanes, decreased by 67 and 57%, respectively ($P < 0.01$) in *ms33* compared to wild type (Fig. 7b, Additional file 2: Table S1). Among cutin components, C16:0 acid, C18:2 acid, C16:0 16-OH acid, C22:0 2-OH acid, and C24:0 2-OH acid are the major types of aliphatic cutin monomers in anthers. The levels of these monomers were substantially reduced (by 71, 71, 53, 70, and 77%, respectively) in *ms33* compared



to wild type (Fig. 7c, Additional file 3: Table S2). These results suggest that MS33 may play an important role in the biosynthesis of wax and cutin monomers, which are essential for normal development of the anther cuticle and pollen grains.

We also compared the total fatty acid levels in wild-type versus *ms33* anthers. Total fatty acids with carbon lengths from C16 to C28 were present at 18.18 $\mu\text{g mg}^{-1}$ in *ms33* anthers but only 9.97 $\mu\text{g mg}^{-1}$ ($P < 0.01$) in wild-type anthers. The levels of the majority of fatty acids increased to various extents in *ms33* (Table 1). However, the octacosanoic acid (C28:0) level in wild-type anthers was 0.05 $\mu\text{g mg}^{-1}$, whereas none was detected in *ms33*. Similarly, eicosanoic acid (C20:0) levels in *ms33* decreased by approximately 20% ($P < 0.01$) compared to wild-type anthers. The differences in fatty acid monomer contents between wild type and *ms33* suggest that MS33 may play an important role in lipid biosynthesis pathways.

MS33 affects the expression of genes involved in wax and cutin biosynthesis

To further elucidate the molecular function of MS33, we conducted high-throughput transcriptome sequencing (RNA-seq) of wild-type and *ms33* anthers at the un-nucleate stage, with three independent biological replicates. The percentages of mapped reads matching unique genomic positions were 71.05 and 70.17% in the wild type and *ms33*, respectively. Based on a false discovery rate (FDR) of < 0.05 , 7953 of 39,604 genes were determined to be differentially expressed between the wild type and *ms33*, including 3335 downregulated and 4618 upregulated genes (Additional file 4: Figure S2a). According to Gene Ontology (GO) enrichment analysis, the downregulated genes are mainly involved in the

categories carbohydrate metabolic process, lipid metabolic process, and fatty acid metabolic process, whereas the upregulated genes are primarily involved in the categories chemical stimulus, organic substance, and hormone stimulus (Additional file 4: Figure S2b). Notably, the DEGs include a number of genes involved in wax and cutin biosynthesis, such as *GLOSSY1*, *ZmFAR1*, and *ZmOCL1* (Additional file 4: Figure S2c) [50, 51], supporting the notion that MS33 functions in anther cuticle and pollen grain development.

Discussion

MS33 is required for anther cuticle and microspore development in maize

Previous studies on male-sterile mutants have shown that normal anther cuticle development is essential for male fertility [9]. The anther cuticle is primarily composed of two lipophilic biopolymers, cutin and wax [52]. Studies on partial depolymerization have demonstrated that cutin is mainly formed through the direct esterification of C16 and C18 fatty acids to glycerol or to each other [42]. Cuticular wax usually consists of aliphatic compounds with a chain length of at least 20 carbons, including alkanes, alcohols, very long chain fatty acids, and esters [34]. In rice and *Arabidopsis*, many enzymes and transcription factors involved in fatty acid biosynthesis also participate in cutin and wax synthesis during anther development. Mutations in these genes often lead to significant reductions in polyester monomer levels in anthers, particularly C16 and C18 monomers [9, 10].

In maize, *MS45*, *MS26*, *IPE1*, and *APV1* are required for anther cuticle development [45, 46]. Defects in these genes result in tapetum degeneration during early microspore development. Similarly, we found that *ms33* anthers had smooth surfaces and severe degradation of the tapetal layer during early microspore development compared with wild-type anthers. The anther cuticle is composed of wax and cuticular cutin, both of which are synthesized in the tapetum [9, 10]. Accordingly, our in situ hybridization showed that *MS33* transcripts were mainly found in the tapetum (Fig. 6b). Furthermore, mutations in *MS33* considerably altered the contents and composition of cutin and wax (Fig. 7). Therefore, we hypothesize that MS33 may be essential for anther cuticle development and that a mutation in *MS33* might alter aliphatic polyester biosynthesis in the tapetum.

To date, many male sterile mutants have been identified to be altered in polyester formation or synthesis of cutin and wax, and they are generally defective in both the anther cuticle and pollen exine, such as *ms2*, *cyp703a2*, and *gpat1 gpat6* double mutant in *Arabidopsis* [20, 36], *dpw*, *osgpat3*, *osnp1*, *cyp703a2*, and *cyp704b2* in rice [9, 10, 34, 37, 53], and *ms45*, *ms26*, *ipe1*, and *apv1* in maize [45, 46]. However, we found no significant structural differences in pollen

Table 1 Total fatty acids in wild-type and *ms33* anthers

Lipids	Wild type $\mu\text{g mg}^{-1}$ dry weight	<i>ms33</i>	Up
C16:1 acid	0.052 \pm 0.009	0.094 \pm 0.008	80.94%
C16:0 acid	4.128 \pm 0.232	7.957 \pm 0.116	92.74%
C18:2 acid	3.976 \pm 0.114	7.786 \pm 0.136	95.85%
C18:3 acid	0.466 \pm 0.018	0.490 \pm 0.012	5.22%
C18:1 acid	0.077 \pm 0.005	0.134 \pm 0.002	73.67%
C18:0 acid	0.531 \pm 0.009	0.808 \pm 0.029	52.17%
C20:0 acid	0.337 \pm 0.015	0.269 \pm 0.016	-20.22%
C22:0 acid	0.195 \pm 0.014	0.345 \pm 0.011	76.72%
C24:0 acid	0.109 \pm 0.008	0.241 \pm 0.005	120.29%
C26:0 acid	0.050 \pm 0.005	0.054 \pm 0.004	7.40%
C28:0 acid	0.053 \pm 0.008	0	-100.00%
Total acids	9.973 \pm 0.399	18.176 \pm 0.257	82.26%

Fatty acid levels shown are means \pm SD ($n = 5$)

exine between wild type and *ms33* at the uninucleate and binucleate stages, although *ms33* microspores had an irregular shape (Additional file 5: Figure S3). There are two possible explanations for these observations. On the one hand, perhaps *MS33* mediates pollen fertility independently because our RNA-seq analysis did not find differential expressions of *MS26*, *MS45*, *IPE1*, and *APV1* between wild type and *ms33* mutants (Additional file 6: Figure S4). On the other hand, perhaps the *ms33* pollen exine has been damaged in a way not detectable by TEM.

The *ms33* mutant displays defective anther cuticle development (Fig. 4). It has been proved that fatty acids are important precursors of cuticular cutin and wax [54]. Metabolism analysis revealed that *ms33* anthers had an increased level of the majority of fatty acids (Table 1). Therefore, we assumed that *ms33* controls cutin and wax metabolism by a complicated feedback regulation. The RNA-seq data are in accordance with this assumption, many genes are involved in fatty acids metabolism, such as fatty acids biosynthesis, fatty acids elongation and fatty acids oxygenation has been up or down regulated (Additional file 4: Figure S2c).

The functions of GPAT family members are conserved and diverse in higher plants

GPAT-catalyzed de novo lipid biosynthesis has been extensively characterized in bacteria, fungi, and animals [55, 56]. In *Arabidopsis*, 10 GPATs have been identified, eight of which are specific to land plants and do not participate in membrane or storage lipid production [8]. Previous in vitro substrate specificity tests and phylogenetic analyses have shown that GPAT4/6/8 and GPAT5/7 are involved in cutin and suberin biosynthesis, respectively [35, 57, 58]. The *gpat4* and *gpat8* mutants exhibit reduced levels of C16 and C18 fatty acids and dicarboxylic acid cutin monomers in stems and leaves [49]. GPAT1/2/3 share a close evolutionary relationship and are expressed at relatively high levels in flowers. However, no obvious phenotype changes were detected in *gpat2* and *gpat3* mutants. AtGPAT2 and AtGPAT3 showed no activity on some fatty acid-CoA substrates [8, 59]. GPAT1 is active on the substrates of unsubstituted acyl-CoAs, including C16:0, C16:1, C18:0, C18:1, and C20:1 [59]. The *gpat1* mutant shows altered pollen coat structure and reduced fertility. GPAT6 is required for the incorporation of several C16 monomers into flower cutin [60]. The *gpat1 gpat6* double mutant exhibits abnormal pollen exine and tapetum structure, resulting in complete pollen abortion [36]. Therefore, GPAT family members may have diverse functions in the same species.

GPATs catalyze the initial step of glycerolipid biosynthesis by promoting the transfer of acyls from acyl-CoA or acyl-ACP to glycerol 3-phosphate at the *sn*-2 hydroxyl

to produce lysophosphatidic acid or monoacylglycerol, which are substrates for the synthesis of several important glycerolipid intermediates for cutin and wax production in plants [35, 61]. Unfortunately, the roles of GPATs in grasses are still unclear. Sixteen putative land-plant-specific GPATs have been identified in the rice genome [8], and 20 homologous genes were found in the maize genome in the current study (Additional file 1: Figure S1). However, to date, only one GPAT, OsGPAT3, has been characterized in rice [37]. In the current study, *MS33*, the first GPAT gene cloned from maize, was classified in the same clade with AtGPAT2/3 and OsGPAT3 based on phylogenetic analysis. The functions of *GPAT2/3* in *Arabidopsis* are still unknown [36]. Mutations in *OsGPAT3* may lead to abnormal tapetum and anther cuticle development, degenerated pollen grains, and reduced cutin and wax levels in rice, which is similar to our observations for *ms33*. In the current study, like *OsGPAT3* in rice, *MS33* transcripts were mainly detected in the tapetum during anther development in maize. The complete male sterility observed in *ms33* suggests that *MS33* plays an essential role in microspore and anther cuticle development. Furthermore, the significant reduction in the levels of the major aliphatic monomers of cutin and wax in *ms33* anthers suggests that *MS33* may be involved in anther cuticle biosynthesis. In addition, our transcriptome analysis revealed the differential expression of multiple genes involved in cutin and wax biosynthesis, including *FAE* and *KCS1* [62], *ZmOCL1* [51], *WSD1* [63], *CER5/WBC12* [64], *CER1* and *CER3* [65], *ZmWri1a*, *ZmWri1b*, and *WRINKLED1* [66–68] (Additional file 4: Figure S2). Therefore, *MS33* in maize appears to share some common functions with GPAT family members in *Arabidopsis* and rice.

In higher plants, acyl-CoA is synthesized in the plastid and transported to the endoplasmic reticulum in cells in the tapetal layer [10]. We propose that in maize, *MS33* may participate in polyester formation following fatty acid biosynthesis during early anther development. However, identification of the direct substrates and exact functions of *MS33* will require further study.

Conclusions

In this study, a male-sterile mutant *sal1*, which is allelic to the classic *ms33* mutant, displays defective anther cuticle development and premature microspore degradation. By a map-based cloning method, we isolated the *MS33* gene, which encodes a putative glycerol-3-phosphate acyltransferase (GPAT). The RNA in situ hybridization study showed that *MS33* was preferentially expressed in the tapetal layer cells during anther development. Using the gas chromatography-mass spectrometry (GC-MS), substantial reduction in wax and cutin were detected in *ms33*

anthers. Accordingly, transcriptomic analysis demonstrated that many genes involved in wax and cutin biosynthesis were differentially expressed in *ms33* mutant. Taken together, our results suggest that *MS33* plays an important role in anther cuticle and microspore development by affecting lipid polyester biosynthesis. These findings provide insights into the function of glycerol-3-phosphate acyltransferase in the lipid polyester biosynthesis pathway and provide a potential male-sterile line for the utilization of heterosis in maize.

Methods

Plant materials

The *sa1* mutant in maize is a spontaneous mutant identified in the field, derived from breeding line HN17. The *ms33-6019*, *ms33-6024*, and *ms33-6038* mutants were obtained from the Maize Genetics Cooperation Stock Center. Two generations of the plants were cultivated per year; the summer generation was grown in an experimental field of China Agricultural University in Beijing, and the winter generation was grown in an experimental field in Sanya, Hainan. The BC₅F₂ population was created by backcrossing *sa1* to inbred line Z58 using linked markers. Morphological comparisons were performed within siblings from the same family in the BC₅F₂ population.

Phenotypic analysis

The phenotypes of whole plants and reproductive organs were recorded using a Nikon E995 digital camera. Anthers from different developmental stages were collected based on anther length and microspore morphology. Phenotypic observations by semi-thin section, scanning electronic microscopy (SEM), and transmission electronic microscopy (TEM) were performed as described previously [10, 69].

Map-based cloning

Two F₂ mapping populations were obtained by crossing the *sa1* mutant with inbred line B73 or Z58, respectively, and positional cloning was carried out using both populations. Male-sterile plants were identified in the field, and genomic DNA was extracted from mature leaves of these plants using the cetyltrimethylammonium bromide method. Bulked segregant analysis [70] was performed using available SSR markers (www.maizgdb.org). Additional InDel markers were developed flanking the region identified by rough mapping [47]. The primer sequences are listed in Additional file 7: Table S3.

Phylogenetic analysis

The full-length amino acid sequences of 10 *Arabidopsis* GPAT proteins were used as queries to identify their homologs in the maize and rice genomes via BLASTP

(<http://ensembl.gramene.org/Tools/Blast>). In total, the sequences of 20 maize GPATs, 17 rice GPATs, and 10 *Arabidopsis* GPATs were used to construct a phylogenetic tree via bootstrap analysis with 1000 replications using MEGA 4.0 software [8].

Real-time qRT-PCR

Tissue samples including leaves, roots, stems, and anthers of various lengths were separated and ground in liquid N₂. Total RNA was extracted using an RNeasy Plant Mini Kit (Qiagen). The RNA was reverse transcribed using an M-MLV Reverse Transcription Kit (Invitrogen), and qPCR was performed using SYBR Green PCR Master Mix (Takara). Three biological replicates and three technical replicates were performed for each procedure. *ZmACTIN1* was used as the internal reference to normalize the expression data. Relative expression levels were calculated according to the 2^{-ΔΔCT} method [71]. The primer sequences are listed in Additional file 7: Table S3.

In situ hybridization

Anthers at various developmental stage were separated according to length and developmental stage. Tissue fixation and in situ hybridization were performed as previously described [72]. The sequences of gene-specific primers are listed in Additional file 7: Table S3.

Analysis of anther wax, cutin, and total fatty acids

Anthers at the uninucleate microspore stage from wild type and *ms33* were separated from stamens and immediately frozen in liquid N₂. To determine the amount of each compound per unit surface area, the ratio of anther weight to surface area was calculated (Additional file 8: Figure S5). The surface area was calculated based on the length and width of the anther in microscopic images, assuming that maize anthers exhibit the standard cylindrical shape. Wax, cutin, and total fatty acid composition were analyzed as described previously [45]. Five biological replicates were performed per genotype.

RNA-seq analysis

Anthers were collected from wild-type and *ms33* plants at the uninucleate microspore stage, with three biological replicates per genotype. Total RNA was isolated with TRIzol reagent (Invitrogen). Sequencing libraries were constructed using a NEBNext Ultra RNA Library Prep Kit for Illumina (NEB, USA) and sequenced (paired-end, 150-bp reads) on a HiSeq 2500 sequencer. The raw data were filtered by removing reads containing adapters, reads containing poly-N, and low-quality reads to obtain at least six gigabases of clean data per sample. The clean data were aligned to the maize genome (AGPv3; MaizeSequence.org) using TopHat v2.0.12 [73]

with default parameters. Gene expression levels were normalized by gene length and read numbers to calculate FPKM values (fragments per kilobase of transcript per million mapped reads). Significant DEGs were identified using the Cufflinks program [74]. The Singular Enrichment Analysis (SEA) tool in AgriGO [75] was utilized for GO enrichment analysis of the DEGs list, with default parameters. The DEGs were classified into functional categories defined by MapMan BINs (mapman.gabipd.org).

Accession numbers

The maize GPAT genes referred to in this article can be found in the MaizeGDB/Gramene database under accession numbers GRMZM2G070304, GRMZM2G020320, GRMZM2G048561, GRMZM2G059637, GRMZM2G064590, GRMZM2G065203, GRMZM2G072298, GRMZM2G075295, GRMZM2G083195, GRMZM2G096010, GRMZM2G116243, GRMZM2G123987, GRMZM2G124042, GRMZM2G131378, GRMZM2G147917, GRMZM2G156729, GRMZM2G159890, GRMZM2G165681, GRMZM2G166176, and GRMZM2G177150.

The rice GPAT genes referred to in this article can be found in the Gramene database under accession numbers Os12g37600, Os11g45400, Os10g41070, Os10g27330, Os08g03700, Os05g38350, Os05g37600, Os05g20100, Os03g61720, Os03g52570, Os02g02340, Os01g63580, Os01g44069, Os01g22560, Os01g19390, Os01g14900, and Os10g42720.

Arabidopsis GPAT sequences can be found in the TAIR data libraries under the following accession numbers: AtATS1 (AT1G32200), AtGPAT1 (AT1G06520), AtGPAT2 (AT1G02390), AtGPAT3 (AT4G01950), AtGPAT4 (AT1G01610), AtGPAT5 (AT3G11430), AtGPAT6 (AT2G38110), AtGPAT7 (AT5G06090), AtGPAT8 (AT4G00400), and AtGPAT9 (AT5G60620).

Additional files

Additional file 1: Figure S1. Phylogenetic analysis of MS33 and related homologs. MEGA 4.0 was used to construct the phylogenetic tree based on the neighbor-joining method. 10 *Arabidopsis* GPAT proteins, 17 rice GPAT proteins, and 20 homologs of MS33 in maize were used for analysis and formed distinct clades. (TIF 796 kb)

Additional file 2: Table S1. Detailed wax compositions in wild-type and *ms33* anthers. (DOCX 15 kb)

Additional file 3: Table S2. Detailed cutin compositions in wild-type and *ms33* anthers. (DOCX 15 kb)

Additional file 4: Figure S2. Heat map representation of the differences in gene expression between the wild type and *ms33*. (a) Volcano plot of significant DEGs. X-axis: \log_2 of the fold change in *ms33*/wild type, Y-axis: $-\log_{10}$ of the adjusted *P*-value. Red and green dots represent significantly up- and down-regulated genes, respectively (FDR < 0.01). Blue dots are genes with no significant change in expression. (b) GO functional categories of genes up- and downregulated in the indicated comparisons. The color of each cell indicates $-\log_{10}$ (*P*-values) of GO enrichment according to the scale shown. (c) Functional

annotation and description of selected DEGs involved in anther cuticle development. For each gene, the FPKM value was normalized by the highest FPKM value of the gene across two samples. (TIF 10741 kb)

Additional file 5: Figure S3. Transmission electron microscopy of pollen exine in the wild type and *ms33*. (a) and (b), early uninucleate stage; (c) and (d), late uninucleate stage; (e) and (f), binucleate stage. Ex, exine. Bar = 500 nm in (a), (b), and (c), 1 μ m in (d), (e) and (f). (TIF 1738 kb)

Additional file 6: Figure S4. MS26, MS45, IPE1, and APV1 transcript levels in the wild type and *ms33*. Error bars indicate SD (*n* = 3). (TIF 9081 kb)

Additional file 7: Table S3. List of primers used in this study. (DOCX 15 kb)

Additional file 8: Figure S5. Weight/surface area ratios of wild type and *ms33* anthers. (TIF 3576 kb)

Abbreviations

bp: base pair; InDel: Insertion/Deletion; qRT-PCR: quantitative real-time polymerase chain reaction; SRA: Sequence read archive; SSR: Simple sequence repeat; TAIR: The Arabidopsis Information Resource

Acknowledgements

The authors thank Dr. Gui Su for providing valuable comments during the preparation of this manuscript and Fengxia Zhang (The Metabolomics Facility of the Institute of Genetics and Developmental Biology, Chinese Academy of Sciences) for wax, cutin, and fatty acid analysis. We also thank the staff of the Maize Genetics Cooperation Stock Center for their help in providing germplasm.

Funding

This research was supported by the National Natural Science Foundation of China (31801375, 91735305, and 31471499).

Availability of data and materials

All sequence reads have been deposited in NCBI Sequence Read Archive (<http://www.ncbi.nlm.nih.gov/sra>). The BioProject and SRA accession numbers are PRJNA437229 and SRP134140, respectively.

Authors' contributions

L.Z., Y.Z., X.C., S.L., M.L., and W.H. performed phenotypic analysis, mapped and cloned MS33, carried out expression analysis, conducted anther wax, cutin, and fatty acid assays, and wrote the article. H.L. provided the *sa1* mutants; Y.H. analyzed the RNA-seq data; S.Y. performed RNA in situ hybridizations; X.Z. edited the manuscript; W.J. contributed to designing the research and edited the manuscript. All authors read and approved the final manuscript.

Ethics approval and consent to participate

Not applicable.

Consent for publication

Not applicable.

Competing interests

The authors declare that they have no competing interests.

Publisher's Note

Springer Nature remains neutral with regard to jurisdictional claims in published maps and institutional affiliations.

Author details

¹National Maize Improvement Center of China, Beijing Key Laboratory of Crop Genetic Improvement, Key Laboratory of Crop Heterosis and Utilization, Ministry of Education (MOE), Center for Crop Functional Genomics and Molecular Breeding, China Agricultural University, Beijing 100193, China. ²College of Agronomy, Southern Regional Collaborative Innovation Center for Grain and Oil Crops, Hunan Agricultural University, Changsha 410128, China. ³Department of Vegetable Sciences, Beijing Key Laboratory of Growth and Developmental Regulation for Protected Vegetable Crops, China Agricultural University, Beijing 100193, China.

Received: 11 March 2018 Accepted: 20 November 2018

Published online: 03 December 2018

References

- Ma H. Molecular genetic analyses of microsporogenesis and microgametogenesis in flowering plants. *Annu Rev Plant Biol.* 2005;56:393–434.
- Zhang D, Luo X, Zhu L. Cytological analysis and genetic control of rice anther development. *J Genet Genomics.* 2011;38:379–90.
- Sanders PM, Bui AQ, Weterings K, McIntire KN, Hsu YC, Lee PY, Truong MT, Beals TP, Goldberg RB. Anther developmental defects in *Arabidopsis thaliana* male-sterile mutants. *Sex Plant Reprod.* 1999;11:297–322.
- Scott RJ, Spielman M, Dickinson HG. Stamen structure and function. *Plant Cell.* 2004;16:S46–60.
- Wang Y WH, Yang M. Microscopy and bioinformatic analyses of lipid metabolism implicate a sporophytic signaling network supporting pollen development in *Arabidopsis*. *Mol Plant.* 2008;1:667–74.
- Kolattukudy PE. Polyesters in higher plants. *Adv Biochem Eng Biotechnol.* 2001;71:1–49.
- Xu J, Ding Z, Vizcay-Barrena G, Shi J, Liang W, Yuan Z, Werck-Reichhart D, Schreiber L, Wilson ZA, Zhang D. ABORTED MICROSPORES acts as a master regulator of pollen wall formation in *Arabidopsis*. *Plant Cell.* 2014;26:1544–56.
- Yang W, Simpson JP, Li-Beisson Y, Beisson F, Pollard M, Ohlrogge JB. A land-plant-specific glycerol-3-phosphate acyltransferase family in *Arabidopsis*: substrate specificity, sn-2 preference, and evolution. *Plant Physiol.* 2012;160:638–52.
- Li H, Zhang D. Biosynthesis of anther cuticle and pollen exine in rice. *Plant signal behave.* 2010;5:1121–3.
- Yang X, Wu D, Shi J, He Y, Pinot F, Grausem B, Yin C, Zhu L, Chen M, Luo Z, Liang W, Zhang D. Rice CYP703A3, a cytochrome P450 hydroxylase, is essential for development of anther cuticle and pollen exine. *J Integr Plant Biol.* 2014;56:979–94.
- Schreiber L. Transport barriers made of cutin, suberin and associated waxes. *Trends Plant Sci.* 2010;15:546–53.
- Heredia A. Biophysical and biochemical characteristics of cutin, a plant barrier biopolymer. *BBA-Gen Subjects.* 2003;1620:1–7.
- Nawrath C. Unraveling the complex network of cuticular structure and function. *Curr Opin Plant Biol.* 2006;9:281–7.
- Beisson F, Li-Beisson Y, Pollard M. Solving the puzzles of cutin and suberin polymer biosynthesis. *Curr Opin Plant Biol.* 2012;15:329–37.
- Fich EA, Segerson NA, Rose JK. The plant polyester Cutin: biosynthesis, structure, and biological roles. *Annu Rev Plant Biol.* 2016;67:207–33.
- Bak S, Beisson F, Bishop G, Hamberger B, Hofer R, Paquette S, Werck-Reichhart D. Cytochromes P450. *Arabidopsis Book.* 2011;9:e0144.
- Kunst L, Samuels L. Plant cuticles shine: advances in wax biosynthesis and export. *Curr Opin Plant Biol.* 2009;12:721–7.
- Yeats TH, Rose JK. The formation and function of plant cuticles. *Plant Physiol.* 2013;163:5–20.
- Wilson ZA, Morrill SM, Dawson J, Swarup R, Tighe PJ. The *Arabidopsis* MALE STERILITY1 (MS1) gene is a transcriptional regulator of male gametogenesis, with homology to the PHD-finger family of transcription factors. *Plant J.* 2001;28:27–39.
- Chen W, Yu XH, Zhang K, Shi J, De Oliveira S, Schreiber L, Shanklin J, Zhang D. Male sterile2 encodes a plastid-localized fatty acyl carrier protein reductase required for pollen exine development in *Arabidopsis*. *Plant Physiol.* 2011;157:842–53.
- Ariizumi T, Hatakeyama K, Hinata K, Sato S, Kato T, Tabata S, Toriyama K. A novel male-sterile mutant of *Arabidopsis thaliana*, faceless pollen-1, produces pollen with a smooth surface and an acetolysis-sensitive exine. *Plant Mol Biol.* 2003;53:107–16.
- Paxson-Sowers DM, Dodrill CH, Owen HA, Makaroff CA. DEX1, a novel plant protein, is required for exine pattern formation during pollen development in *Arabidopsis*. *Plant Physiol.* 2001;127:1739–49.
- Ariizumi T, Hatakeyama K, Hinata K, Inatsugi R, Nishida I, Sato S, Kato T, Tabata S, Toriyama K. Disruption of the novel plant protein NEF1 affects lipid accumulation in the plastids of the tapetum and exine formation of pollen, resulting in male sterility in *Arabidopsis thaliana*. *Plant J.* 2004;39:170–81.
- Morant M, Jorgensen K, Schaller H, Pinot F, Lindberg Moller B, Werck-Reichhart D, Bak S. CYP703 is an ancient cytochrome P450 in land plants catalyzing in-chain hydroxylation of lauric acid to provide building blocks for sporopollenin synthesis in pollen. *Plant Cell.* 2007;19:1473–87.
- de Azevedo Souza C, Kim SS, Koch S, Kienow L, Schneider K, McKim SM, Haughn GW, Kombrink E, Douglas CJ. A novel fatty acyl-CoA Synthetase is required for pollen development and sporopollenin biosynthesis in *Arabidopsis*. *Plant Cell.* 2009;21:507–25.
- Dobritsa AA, Shrestha J, Morant M, Pinot F, Matsuno M, Swanson R, Møller BL, Preuss D. CYP704B1 is a long-chain fatty acid ω -hydroxylase essential for sporopollenin synthesis in pollen of *Arabidopsis*. *Plant Physiol.* 2009;151:574–89.
- Zhang D, Liang W, Yuan Z, Li N, Shi J, Wang J, Liu Y, Yu WJ, Zhang D. Tapetum degeneration retardation is critical for aliphatic metabolism and gene regulation during rice pollen development. *Mol Plant.* 2008;1:599–610.
- Kaneko M, Inukai Y, Ueguchi-Tanaka M, Itoh H, Izawa T, Kobayashi Y, Hattori T, Miyao A, Hirochika H, Ashikari M, Matsuoka M. Loss-of-function mutations of the rice *GAMYB* gene impair alpha-amylase expression in aleurone and flower development. *Plant Cell.* 2004;16:33–44.
- Hu L, Tan H, Liang W, Zhang D. The post-meiotic Deficient Anther1 (PDA1) gene is required for post-meiotic anther development in rice. *J Genet Genomics.* 2010;37:37–46.
- Li H, Yuan Z, Vizcay-Barrena G, Yang C, Liang W, Zong J, Wilson ZA, Zhang D. PERSISTENT TAPETAL CELL1 encodes a PHD-finger protein that is required for tapetal CELL death and pollen development in rice. *Plant Physiol.* 2011;156:615–30.
- Zhang D, Liang W, Yin C, Zong J, Gu F, Zhang D. OsC6, encoding a lipid transfer protein, is required for postmeiotic anther development in rice. *Plant Physiol.* 2010;154:149–62.
- Jung KH, Han MJ, Lee DY, Lee YS, Schreiber L, Franke R, Faust A, Yephremov A, Saedler H, Kim YW, Hwang I, An G. Wax-deficient anther1 is involved in cuticle and wax production in rice anther walls and is required for pollen development. *Plant Cell.* 2006;18:3015–32.
- Li H, Pinot F, Sauveplane V, Werck-Reichhart D, Diehl P, Schreiber L, Franke R, Zhang P, Chen L, Gao Y, Liang W, Zhang D. Cytochrome P450 family member CYP704B2 catalyzes the ω -hydroxylation of fatty acids and is required for anther cutin biosynthesis and pollen exine formation in rice. *Plant Cell.* 2010;22:173–90.
- Liu Z, Lin S, Shi J, Yu J, Zhu L, Yang X, Zhang D, Liang W. Rice no pollen 1 (NP1) is required for anther cuticle formation and pollen exine patterning. *Plant J.* 2017;91:263–77.
- Yang W, Pollard M, Li-Beisson Y, Beisson F, Feig M, Ohlrogge J. A distinct type of glycerol-3-phosphate acyltransferase with sn-2 preference and phosphatase activity producing 2-monoacylglycerol. *Proc Natl Acad Sci U S A.* 2010;107:12040–5.
- Li X, Zhu J, Yang J, Zhang G, Xing W, Zhang S, Yang Z. Glycerol-3-phosphate acyltransferase 6 (GPAT6) is important for tapetum development in *Arabidopsis* and plays multiple roles in plant fertility. *Mol Plant.* 2012;5:131–42.
- Men X, Shi J, Liang W, Zhang Q, Lian G, Quan S, Zhu L, Chen M, Zhang D. Glycerol-3-phosphate acyltransferase 3 (OsGPAT3) is required for anther development and male fertility in rice. *J Exp Bot.* 2017;68:513–26.
- Timofejeva L, Skibbe DS, Lee S, Golubovskaya I, Wang R, Harper L, Walbot V, Candé WZ. Cytological characterization and allelism testing of anther developmental mutants identified in a screen of maize male sterile lines. G3 (Bethesda). 2013;3:231–49.
- Albertsen MC, Fox TW, Huffman G, Trimmell M. Nucleotide sequences affecting plant male fertility and methods of using same. August 29, 2006. United States patent application no. 7098388B2.
- Albertsen MC, Fox TW, Trimmell MR. Cloning and utilizing a maize nuclear male sterility gene. *Proc Ann Corn Sorghum Res Conf.* 1993;48:224–33.
- Djukanovic V, Smith J, Lowe K, Yang M, Gao H, Jones S, Nicholson MG, West A, Lape J, Bidney D, Carl Falco S, Jantz D, Alexander Lyznik L. Male-sterile maize plants produced by targeted mutagenesis of the cytochrome P450-like gene (MS26) using a redesigned I-CreI homing endonuclease. *Plant J.* 2013;76:888–99.
- Graca J, Lamosa P. Linear and branched poly(ω -hydroxyacid) esters in plant cutins. *J Agric Food Chem.* 2010;58:9666–74.
- Cigan AM, Unger E, Xu R, Kendall T, Fox TW. Phenotypic complementation of ms45 maize requires tapetal expression of MS45. *Sex Plant Reprod.* 2001;14:135–42.
- Skibbe DS, Schnable PS. Male sterility in maize. *Maydica.* 2005;50:367–76.
- Chen X, Zhang H, Sun H, Luo H, Zhao L, Dong Z, Yan S, Zhao C, Liu R, Xu C, Li S, Chen H, Jin W. Irregular pollen Exine1 is a novel factor in anther cuticle and pollen exine formation. *Plant Physiol.* 2017;173:307–25.

46. Somaratne Y, Tian Y, Zhang H, Wang M, Huo Y, Cao F, Zhao L, Chen H. Abnormal pollen Vacuolation1 (APV1) is required for male fertility by contributing to anther cuticle and pollen exine formation in maize. *Plant J*. 2017;90:96–110.
47. Dong Z, Jiang C, Chen X, Zhang T, Ding L, Song W, Luo H, Lai J, Chen H, Liu R, Zhang X, Jin W. Maize LAZY1 mediates shoot gravitropism and inflorescence development through regulating auxin transport, auxin signaling, and light response. *Plant Physiol*. 2013;163:1306–22.
48. Trimnell MR, Patterson E, Fox TW, Bedinger P, Albertsen MC. New chromosome 2L male-sterile mutant ms33 and alleles. *Maize Genetics Cooperation Newsletter*. 1999;73:48–9.
49. Li Y, Beisson F, Koo AJK, Molina I, Pollard M, Ohlrogge J. Identification of acyltransferases required for cutin biosynthesis and production of cutin with suberin-like monomers. *Proc Natl Acad Sci U S A*. 2007;104:18339–44.
50. Sturaro M, Hartings H, Schmelzer E, Velasco R, Salamini F, Motto M. Cloning and characterization of GLOSSY1, a maize gene involved in cuticle membrane and wax production. *Plant Physiol*. 2005;138:478–89.
51. Javelle M, Vernoud V, Depege-Fargeix N, Arnould C, Oursel D, Domergue F, Sarda X, Rogowsky PM. Over-expression of the epidermis-specific HD-ZIP IV transcription factor OCL1 in maize identifies target genes involved in lipid metabolism and cuticle biosynthesis. *Plant Physiol*. 2010;154:273–86.
52. Chang Z, Chen Z, Yan W, Xie G, Lu J, Wang N, Lu Q, Yao N, Yang G, Xia J, Tang X. An ABC transporter, OsABCG26, is required for anther cuticle and pollen exine formation and pollen-pistil interactions in rice. *Plant Sci*. 2016; 253:21–30.
53. Shi J, Tan H, Yu X, Liu Y, Liang W, Ranathunge K, Franke RB, Schreiber L, Wang Y, Kai G, Shanklin J, Ma H, Zhang D. Defective pollen wall is required for anther and microspore development in rice and encodes a fatty acyl carrier protein reductase. *Plant Cell*. 2011;23:2225–46.
54. Shi J, Cui M, Yang L, Kim YJ, Zhang D. Genetic and biochemical mechanisms of pollen wall development. *Trends Plant Sci*. 2015;20:741–53.
55. Murata N, Tasaka Y. Glycerol-3-phosphate acyltransferase in plants. *Biochim Biophys Acta*. 1997;1348:10–6.
56. Zheng Z, Zou J. The initial step of the glycerolipid pathway - identification of glycerol 3-phosphate/dihydroxyacetone phosphate dual substrate acyltransferases in *Saccharomyces cerevisiae*. *J Biol Chem*. 2001;276:41710–6.
57. Beisson F, Li Y, Bonaventure G, Pollard M, Ohlrogge JB. The acyltransferase GPAT5 is required for the synthesis of suberin in seed coat and root of *Arabidopsis*. *Plant Cell*. 2007;19:351–68.
58. Boyce K. The evolutionary history of roots and leaves. In: Holbrook M, Zwieniecki M, editors. *Vascular transport in plants*. Elsevier academic press, Burlington; 2005. p. 479–99.
59. Zheng Z, Xia Q, Dauk M, Shen W, Selvaraj G, Zou JT. *Arabidopsis* AtGPAT1, a member of the membrane-bound glycerol-3-phosphate acyltransferase gene family, is essential for tapetum differentiation and male fertility. *Plant Cell*. 2003;15:1872–87.
60. Li-Beisson Y, Pollard M, Sauveplane V, Pinot F, Ohlrogge J, Beisson F. Nanoridges that characterize the surface morphology of flowers require the synthesis of cutin polyester. *Proc Natl Acad Sci U S A*. 2009;106:22008–13.
61. Chen X, Snyder C, Truksa M, Shah S, Weselake R. Sn-Glycerol-3-phosphate acyltransferases in plants. *Plant Signal Behav*. 2011;6:1695–9.
62. Blacklock BJ, Jaworski JG. Substrate specificity of *Arabidopsis* 3-ketoacyl-CoA synthases. *Biochem and Biophys Res Commun*. 2006;346:583–90.
63. Li F, Wu X, Lam P, Zheng H, Samuels L, Jetter R, Kunst L. Identification of the wax ester synthase/acyl-coenzyme a: diacylglycerol acyltransferase WSD1 required for stem wax ester biosynthesis in *Arabidopsis*. *Plant Physiol*. 2008;148:97–107.
64. Pighin JA, Zheng H, Balakshin LJ, Goodman IP, Western TL, Jetter R, Kunst L, Samuels AL. Plant cuticular lipid export requires an ABC transporter. *Science*. 2004;306:702–4.
65. Bernard A, Domergue F, Pascal S, Jetter R, Renne C, Faure JD, Haslam RP, Napier JA, Lessere R, Joubes J. Reconstitution of plant alkane biosynthesis in yeast demonstrates that *Arabidopsis* ECERIFERUM1 and ECERIFERUM3 are core components of a very-long-chain alkane synthesis complex. *Plant Cell*. 2012;24:3106–18.
66. Cernac A, Benning C. WRINKLED1 encodes an AP2/EREB domain protein involved in the control of storage compound biosynthesis in *Arabidopsis*. *Plant J*. 2004;40:575–85.
67. Maeo K, Tokuda T, Ayame A, Mitsui N, Kawai T, Tsukagoshi H, Ishiguro S, Nakamura K. An AP2-type transcription factor, WRINKLED1, of *Arabidopsis thaliana* binds to the AW-box sequence conserved among proximal upstream regions of genes involved in fatty acid synthesis. *Plant J*. 2009;60: 476–87.
68. Pouvreau B, Baud S, Vernoud V, Morin V, Py C, Gendrot G, Pichon JP, Rouster J, Paul W, Rogowsky PM. Duplicate maize Wrinkled1 transcription factors activate target genes involved in seed oil biosynthesis. *Plant Physiol*. 2011;156:674–86.
69. Moon J, Skibbe D, Timofejeva L, Wang CJR, Kelliher T, Kremling K, Walbot V, Cande WZ. Regulation of cell divisions and differentiation by MALE STERILITY32 is required for anther development in maize. *Plant J*. 2013;76: 592–602.
70. Michelmore RW, Paran I, Kesseli RV. Identification of makers linked to disease-resistance genes by bulked segregant analysis - a rapid method to detect markers in specific genomic regions by using segregating populations. *Proc Natl Acad Sci U S A*. 1991;88:9828–32.
71. Livak KJ, Schmittgen TD. Analysis of relative gene expression data using real-time quantitative PCR and the 2(T)(-Delta Delta C) method. *Methods*. 2001;25:402–8.
72. Zhang X, Madi S, Borsuk L, Nettleton D, Elshire RJ, Buckner B, Janick-Buckner D, Beck J, Timmermans M, Schnable PS, Scanlon MJ. Laser microdissection of narrow sheath mutant maize uncovers novel gene expression in the shoot apical meristem. *PLoS Genet*. 2007;3:1040–52.
73. Trapnell C, Pachter L, Salzberg SL. TopHat: discovering splice junctions with RNA-seq. *Bioinformatics*. 2009;25:1105–11.
74. Trapnell C, Williams BA, Pertea G, Mortazavi A, Kwan G, van Baren MJ, Salzberg SL, Wold BJ, Pachter L. Transcript assembly and quantification by RNA-Seq reveals unannotated transcripts and isoform switching during cell differentiation. *Nat Biotechnol*. 2010;28:511–5.
75. Du Z, Zhou X, Ling Y, Zhang Z, Su Z. agriGO: a GO analysis tool kit for the agricultural community. *Nucleic Acids Res*. 2010;38:64–70.

Ready to submit your research? Choose BMC and benefit from:

- fast, convenient online submission
- thorough peer review by experienced researchers in your field
- rapid publication on acceptance
- support for research data, including large and complex data types
- gold Open Access which fosters wider collaboration and increased citations
- maximum visibility for your research: over 100M website views per year

At BMC, research is always in progress.

Learn more biomedcentral.com/submissions

